Passively Q-switched self-frequency-doubled $Nd^{3+}:GdCa_4O(BO_3)_3$ laser

Xingyu Zhang, Shengzhi Zhao, and Qingpu Wang

Department of Optics, Shandong University, Jinan 250100, China

Shujun Zhang, Lianke Sun, Xunmin Liu, Shaojun Zhang, and Huanchu Chen

State Key Laboratory of Crystal Materials, Jinan 250100, China

Received July 20, 2000; revised manuscript received December 19, 2000

The performance of a flash-lamp-pumped self-frequency-doubled $Nd^{3+}:GdCa_4O(BO_3)_3$ (Nd:GdCOB) laser that is passively Q switched with Cr^{4+}:YAG saturable absorbers is demonstrated. The maximum 0.53-μm pulse energy obtained is 2.6 mJ, and the maximum peak intensity is 15 MW/cm^2. The dependence of the pulse characteristics on the orientation of the saturable absorber and on the cavity length is measured. Meanwhile, the transversal distribution of the intracavity photon density is taken into account in the rate equations for an intracavity frequency-doubled passively Q-switched laser, and the solutions are used to account for the behavior of the passively Q-switched Nd:GdCOB laser.

OCIS codes: 140.3380, 140.3430, 140.3460, 140.3530, 140.3540, 140.3580.

1. INTRODUCTION

$Nd^{3+}:GdCa_4O(BO_3)_3$ (Nd:GdCOB) is a new self-activating and self-frequency-doubling (SFD) laser crystal.[1–6] Compared with the old SFD crystal $Nd_xY_{1-x}Al_3(BO_3)_4$, it has the advantages of having a high damage threshold, a high nonlinear coefficient, and low self-absorption at the second-harmonic wavelength and of being easy to grow to a large size by the Czochralski technique. It has several absorption peaks in the range 300–900 nm,[1–4] and therefore it is suitable for Ti:sapphire pumping,[1,2,5] diode pumping,[3,6] and flash-lamp pumping. Two phase-matching directions at which the efficient self-frequency doubling has been realized have been reported. One lies in the XY principal plane ($\theta = 90°$, $\varphi = 46°$),[1–3,6] and the other is out of the principal planes ($\theta = 66.8°$, $\varphi = 132.6°$).[4,5] With Ti:sapphire pumping and the phase-matching direction lying out of the principal planes, a 225-mW 0.53-μm laser was obtained at an absorbed pump power of 1.56 W.[5] With diode pumping and the phase-matching direction lying in the XY principal plane, a 115-mW 0.53-μm laser was obtained at an absorbed pump power of 1.25 W.[3] By use of an acousto-optic modulator as the Q switch inside the cavity, 0.53-μm pulses with an energy of 8.5 μJ, a width of 300 ns, and a repetition rate of 50 kHz were obtained.[6]

In this paper we report on the performance of a xenon flash-lamp-pumped SFD Nd:GdCOB laser passively Q switched with Cr^{4+}:YAG saturable absorbers. When the initial transmission of the Cr^{4+}:YAG saturable absorber is $T_0 = 88\%$ and the cavity length is $L_e = 48$ cm, 0.53-μm pulses with an energy of 2.6 mJ and a width of 112 ns are obtained. When $T_0 = 88\%$ and $L_e = 24$ cm, the pulse energy is 2.1 mJ, the pulse width is 71 ns, and the corresponding peak power and peak intensity are, respectively, 29 kW and 15 MW/cm^2 (the beam radius at the waist is 0.25 mm). The dependences of the pulse characteristics on the orientation of the saturable absorber and on the cavity length are measured and compared with theory.

Rate equations are efficacious tools for analyzing the performance of a Q-switched laser.[7,8] By addition of a term to represent the loss that is due to second-harmonic generation (SHG) to the photon-density equation, the characteristics of the fundamental-frequency and second-harmonic pulses of intracavity frequency-doubled actively Q-switched lasers[9,10] and passively Q-switched lasers[11,12] have been described. However, the rate equations mentioned above are obtained under a plane-wave approximation, which assumes that the intracavity photon density and the population inversion density within the beam cross section depend only on time and that the beam cross section of the second harmonic is equal to that of the fundamental. Actually, this assumption is not properly satisfied because the fundamental is a Gaussian transversal distribution for the TEM_{00} mode and the beam radius of the second harmonic is smaller than that of the fundamental. Recently the transversal distributions of the intracavity photon density and the population inversion density in the rate equations of actively Q-switched lasers[13] and of passively Q-switched lasers[14] (not intracavity frequency-doubled lasers) have been considered and the importance of these distributions has been shown. Therefore, for a more accurate theoretical analysis of the pulses from an intracavity frequency-doubled Q-switched laser it is desirable to consider the transversal variations of the intracavity photon density and the population inversion density in the rate equations.

In this paper we consider the transversal distributions of the intracavity photon density and the population inversion density in the rate equations of intracavity frequency-doubled passively Q-switched lasers, and use

0740-3224/2001/060770-10$15.00

the solutions to account for the behavior of the passively Q-switched Nd:GdCOB laser. In deriving the rate equations we first consider a general intracavity frequency-doubled passively Q-switched laser and then simplify the equations according to the specific properties of the laser with a view to making the resultant rate equations broadly usable.

2. EXPERIMENT AND RESULTS

The experimental setup is shown schematically in Fig. 1. The resonator is a concave–concave cavity. Both of the concave mirrors have a 150-cm radius of curvature, and both are coated for high reflectance at 1.06 μm and high transmission at 0.53 μm. The Nd:GdCOB crystal ($3\ \text{mm} \times 3\ \text{mm} \times 22\ \text{mm}$) is cut for type I phase matching at $\theta = 66.8°$ and $\varphi = 132.6°$ and is antireflection coated at both 1.06 and 0.53 μm on its two flat ends. It is pumped by a pulsed xenon flash lamp with an effective length of 40 mm, and the laser head is located in the center of the cavity. The Cr^{4+}:YAG saturable absorber, antireflection coated at 1.06 μm, is placed close to cavity mirror M1, and the laser light propagates along the [001] crystallographic axis.[15] Two Cr^{4+}:YAG saturable absorbers with initial transmissions of 88% and 91%, are used in the experiment. Two filters are used to block the residual 1.06-μm laser that escapes from the cavity mirrors whose reflectivities at this wavelength are not exactly 100%, and an MRD500 PIN detector (0.5-ns response time, Institute of Semiconductors, Chinese Academy of Sciences) and a Tektronix TDS620B digital oscilloscope (500-MHz bandwidth) are used to receive and display the pulses. The pulse energy is measured with two LPE-1B energy meters (Institute of Semiconductors, Chinese Academy of Sciences).

The pump pulse duration is ~90 μs. The threshold pump energies that correspond to the two Cr^{4+}:YAG saturable absorbers are 8.0 and 6.3 J. In the experiment we set the pump energies slightly higher than the threshold pump energies (8.6 and 6.8 J), and thus only one Q-switched pulse is generated in each pump pulse.

The 0.53-μm pulses and the residual 1.06-μm pulses are found to be strongly linearly polarized and orthogonal to each other. When the Cr^{4+}:YAG saturable absorber rotates on the laser axis (i.e., the [001] crystallographic axis of the saturable absorber), the polarization directions of the pulses of the two wavelengths remain unchanged. This shows that the polarization directions of the oscillating fundamental and the second harmonic are determined by the Nd:GdCOB crystal.

For a given cavity length L_e and a given saturable-absorber initial transmission T_0, when the Cr^{4+}:YAG saturable absorber rotates on the laser axis the 0.53-μm pulse energy and width also change. The maximum pulse energy is obtained when the polarization direction of the fundamental is coincident with the [010] crystallographic axis of the saturable absorber. Figures 2 and 3 show the variations in pulse energy and width with rotation angle δ for $L_e = 36\ \text{cm}$ and $T_0 = 88\%$ and $T_0 = 91\%$, respectively, where δ is measured with respect to the orientation for generating the maximum pulse energy and pulse energy means the total energy received by energy meters EM1 and EM2.

The 0.53-μm pulse energy and width also depend on cavity length L_e. Figures 4 and 5 show the variations of pulse energy and pulse width with L_e when the saturable absorbers are in their optimal orientation. In Figs. 2–5 the filled circles are the experimental results and the solid curves are the theoretical results, which we explain in detail in Section 3 below. Figure 6 is a typical 0.53-μm pulse obtained when $T_0 = 88\%$ and $L_e = 36\ \text{cm}$.

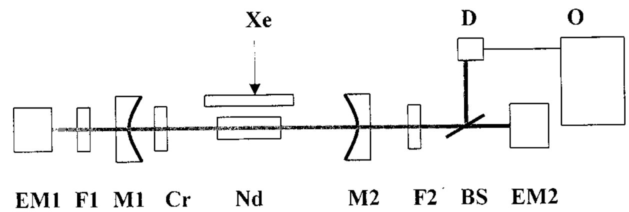

Fig. 1. Schematic of the experimental setup: M1, M2, cavity mirrors; Cr, Cr^{4+}:YAG saturable absorber; Nd, Nd:GdCOB crystal; Xe, xenon flash lamp; F1, F2, filters; BS, beam splitter; EM1, EM2, energy meters; D, detector; O, oscilloscope.

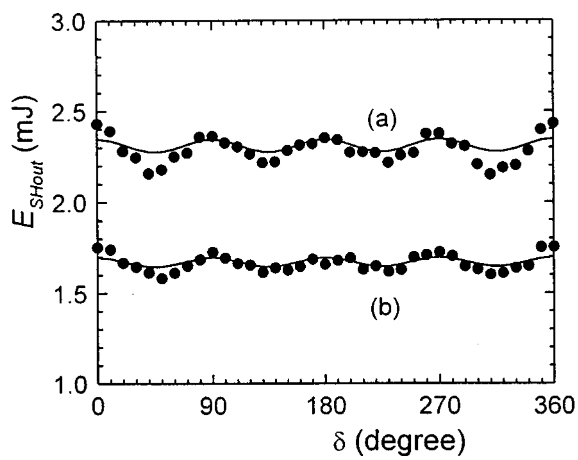

Fig. 2. Relation between the pulse energy and the rotation angle δ of the saturable absorber for cavity length $L_e = 36\ \text{cm}$; δ is measured with respect to the orientation for generating the maximum pulse energy. Filled circles, experimental results; curves, theoretical results: (a) the initial transmission of the saturable absorber, $T_0 = 88\%$, and (b) $T_0 = 91\%$.

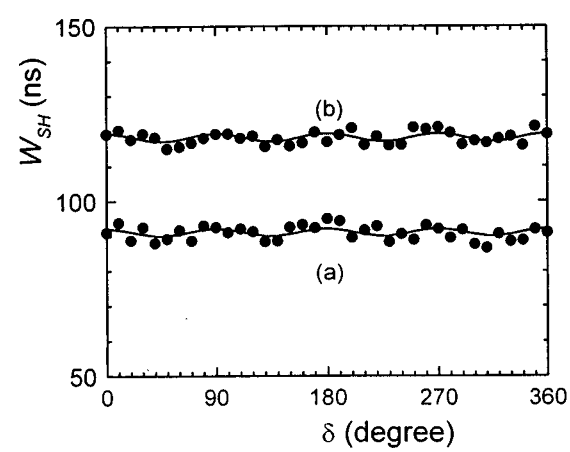

Fig. 3. Relation between the pulse width and the rotation angle δ of the saturable absorber for $L_e = 36\ \text{cm}$. Filled circles, experimental results; curves, theoretical results: (a) $T_0 = 88\%$, (b) $T_0 = 91\%$.

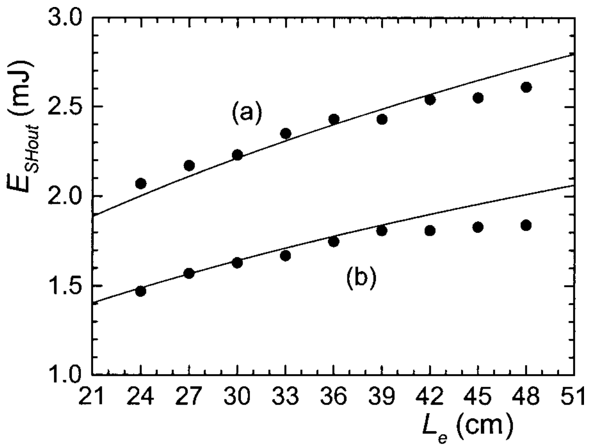

Fig. 4. Relation between pulse energy and cavity length L_e. Filled circles, experimental results; curves, theoretical results: (a) $T_0 = 88\%$, (b) $T_0 = 91\%$.

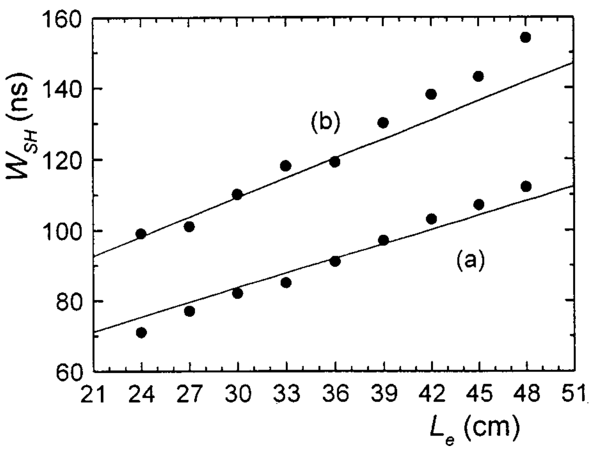

Fig. 5. Relation between pulse width and cavity length L_e. Filled circles, experimental results; curves, theoretical results: (a) $T_0 = 88\%$, (b) $T_0 = 91\%$.

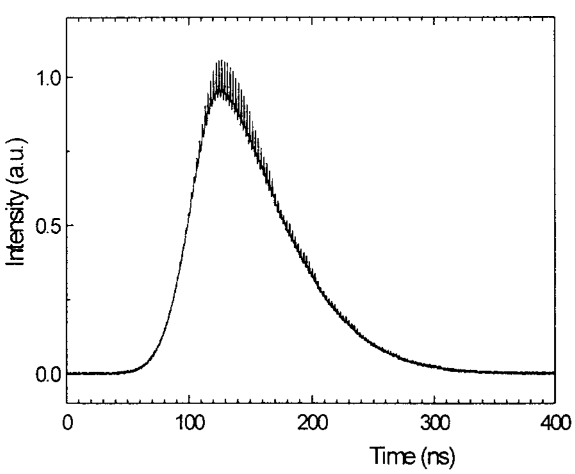

Fig. 6. Typical pulse obtained for $T_0 = 88\%$ and $L_e = 36$ cm.

Because only one Q-switched pulse is generated in each pump pulse, the repetition rate of the Q-switched pulses is equal to that of the pump pulses, which can be 1, 2, 5, or 10 Hz. The above results are obtained for a repetition rate of 1 Hz. When the repetition rate becomes higher, the 0.53-μm pulse energy becomes slightly smaller and the pulse width becomes slightly larger.

When $T_0 = 88\%$ and $L_e = 48$ cm and the saturable absorber is in its optimal orientation, we obtain 0.53-μm pulses with an energy of 2.6 mJ and a pulse width of 112 ns. When $T_0 = 88\%$ and $L_e = 24$ cm, the pulse energy is 2.1 mJ, the pulse width is 71 ns, and the corresponding peak power and peak intensity are, respectively, 29 kW and 15 MW/cm^2 (the beam radius at the waist is 0.25 mm).

When there is no Cr^{4+}:YAG saturable absorber in the cavity at the pump energy of 8.6 J, the 0.53-μm light energy is 0.3 mJ, and the time range of the spikes is 50 μs, the corresponding laser intensity is 3.1 kW/cm^2. The 0.53-μm pulse peak intensity of the passively Q-switched SFD Nd:GdCOB laser is 4.8×10^3 times larger than that of the free-running laser under the same pumping conditions. Obviously this increase is attributable to the high peak intensity of the Q-switched 1.06-μm pulses, for the 1.06–0.53 μm conversion efficiency increases with the 1.06-μm laser peak intensity.

3. THEORETICAL ANALYSIS AND DISCUSSION

A. Loss Rate of the Fundamental Caused by Second-Harmonic Generation

When a laser beam with an intensity $I_F(r, t)$ (where r is the radial coordinate and t is the time) passes through a nonlinear crystal with length l_n, the second-harmonic (SH) intensity $I_{SH}(r, t)$ can be written as[16]

$$I_{SH}(r, t) = I_F(r, t)\tanh^2[\eta^{1/2} I_F^{1/2}(r, t)], \tag{1}$$

where η is a parameter to mark the ability of the nonlinear crystal to convert the fundamental to the SH, which can be written as

$$\eta = 2 l_n^{\,2} \omega^2 d_{\text{eff}}^{\,2} \left(\frac{\mu_0}{\epsilon_r \epsilon_0} \right)^{3/2} \frac{\sin^2(l_n \Delta k/2)}{(l_n \Delta k/2)^2}, \tag{2}$$

where ω is the frequency of the fundamental, $d_{\text{eff}}[\text{A s/V}^2]$ is the effective nonlinear coefficient of the nonlinear crystal, μ_0 and ϵ_0 are the permeability and permittivity of free space, respectively, ϵ_r is the relative permittivity of the nonlinear crystal, and Δk is the phase mismatch.

For a laser operating in the TEM_{00} mode, the intracavity photon density $\phi(r, t)$ (in free space) can be written as

$$\phi(r, t) = \phi(0, t)\exp\left(-\frac{2r^2}{\omega_L^{\,2}} \right), \tag{3}$$

where $\phi(0, t)$ is the photon density in the laser axis and ω_L is the laser mode radius, which, as determined mainly by the geometry of the resonator, may be a function of the longitudinal coordinate z. If so, ω_L in Eq. (3) means the laser mode radius at the position of the gain medium and $\phi(r, t)$ means the equivalent photon density in free space at the position of the gain medium (the actual photon density in the gain medium is r_g times as much as that in free space at the same position, where r_g is the refractive index of the gain medium). As in other treatments,[7–14] the standing-wave effects are ignored; that is to say, $\int_0^\infty \phi(r, t) 2\pi r dr$ can be considered to be independent of z.

Considering that the Q-switched pulse width is long compared with the round-trip time of the cavity and that the fundamental propagates in two opposite directions in the cavity, the relation between the intracavity photon density $\phi(r, t)$ and the unidirectional intensity of the fundamental $I_F(r, t)$ can be written as

$$I_F(r, t) = chv\phi(r, t)/2, \tag{4}$$

where c is the speed of light in vacuum and hv is the photon energy of the fundamental.

By using Eqs. (1) and (4) we can write the total round-trip power of the SH as

$$\begin{aligned} P_{\mathrm{SH}}(t) &= 2\int_0^\infty I_{\mathrm{SH}}(r, t)2\pi r\mathrm{d}r \\ &= chv\int_0^\infty \phi(r, t) \\ &\quad\times \tanh^2[\eta^{1/2}(chv/2)^{1/2}\phi^{1/2}(r, t)]2\pi r\mathrm{d}r. \end{aligned} \tag{5}$$

As $P_{\mathrm{SH}}(t)$ is converted from the fundamental, the loss rate of the fundamental-frequency photon density caused by SHG, $\mathrm{d}\phi(r, t)/\mathrm{d}t|_{\mathrm{SHG}}$, satisfies the following relation:

$$P_{\mathrm{SH}}(t) = hvl'\int_0^\infty \left.\frac{\mathrm{d}\phi(r, t)}{\mathrm{d}t}\right|_{\mathrm{SHG}} 2\pi r\mathrm{d}r, \tag{6}$$

where l' is the optical length of the cavity.

By using Eqs. (5) and (6) we obtain

$$\int_0^\infty \left.\frac{\mathrm{d}\phi(r, t)}{\mathrm{d}t}\right|_{\mathrm{SHG}} 2\pi r\mathrm{d}r = \int_0^\infty \frac{2\phi(r, t)}{t_r}\tanh^2[\eta^{1/2}(chv/2)^{1/2}\phi^{1/2}(r, t)]2\pi r\mathrm{d}r, \tag{7}$$

where t_r is the round-trip transit time of light in the cavity, which can be written as

$$t_r = \frac{2(r_g l + r_s l_s + L_e - l - l_s)}{c}, \tag{8}$$

where L_e, l, and l_s are, respectively, the lengths of the cavity, the gain medium, and the saturable absorber and r_g and r_s are, respectively, the refractive indices of the gain medium and of the saturable absorber.

B. General Rate Equations

By adding a term representing the loss of the fundamental-frequency photon density caused by SHG into the rate equations in Ref. 14 and considering the transmission anisotropy in the saturation regime of the saturable absorber,[18–21] we obtain the following rate equations for intracavity frequency-doubled passively Q-switched lasers:

$$\begin{aligned} \int_0^\infty &\frac{\mathrm{d}\phi(r, t)}{\mathrm{d}t} 2\pi r\mathrm{d}r \\ &= \int_0^\infty \frac{\phi(r, t)}{t_r}[2\sigma n(r, t)l - \ln(1/R) - L]2\pi r\mathrm{d}r \\ &\quad - \cos^2\zeta\int_0^\infty \frac{\phi(r, t)}{t_r}\{2\sigma_{\mathrm{gsa}}n_{\mathrm{sg}}{}^{(1)}(r, t)l_s \\ &\quad + 2\sigma_{\mathrm{esa}}[n_{s0} - n_{\mathrm{sg}}{}^{(1)}(r, t)]l_s\}2\pi r\mathrm{d}r \\ &\quad - \sin^2\zeta\int_0^\infty \frac{\phi(r, t)}{t_r}\{2\sigma_{\mathrm{gsa}}n_{\mathrm{sg}}{}^{(2)}(r, t)l_s + 2\sigma_{\mathrm{esa}} \\ &\quad \times [n_{s0} - n_{\mathrm{sg}}{}^{(2)}(r, t)]l_s\}2\pi r\mathrm{d}r \\ &\quad - \int_0^\infty \frac{2\phi(r, t)}{t_r}\tanh^2[\eta^{1/2}(chv/2)^{1/2}\phi^{1/2}(r, t)]2\pi r\mathrm{d}r, \end{aligned} \tag{9}$$

$$\frac{\mathrm{d}n(r, t)}{\mathrm{d}t} = -\gamma\sigma c\phi(r, t)n(r, t), \tag{10}$$

$$\frac{\mathrm{d}n_{\mathrm{sg}}{}^{(1)}(r, t)}{\mathrm{d}t} = -\frac{S_g}{S_s}\sigma_{\mathrm{gsa}}c\phi(r, t)n_{\mathrm{sg}}{}^{(1)}(r, t)\cos^2\zeta, \tag{11}$$

$$\frac{\mathrm{d}n_{\mathrm{sg}}{}^{(2)}(r, t)}{\mathrm{d}t} = -\frac{S_g}{S_s}\sigma_{\mathrm{gsa}}c\phi(r, t)n_{\mathrm{sg}}{}^{(2)}(r, t)\sin^2\zeta, \tag{12}$$

where $n(r, t)$ is the population inversion density; $n_{\mathrm{sg}}{}^{(1)}(r, t)$ and $n_{\mathrm{sg}}{}^{(2)}(r, t)$ are the ground-state population densities of the Cr^{4+} groups [010] and [100], respectively; n_{s0} is the total population density of the Cr^{4+} in one group; σ is the stimulated-emission cross section of the gain medium; σ_{gsa} and σ_{esa} are, respectively, the ground-state and excited-state absorption cross sections of the saturable absorber; ζ is the angle between the polarization of the fundamental determined by the Nd:GdCOB crystal and the Cr^{4+}:YAG [010] crystallographic axis ($\zeta = -\delta$); R is the product of the reflectivities of the two cavity mirrors at the fundamental frequency (which is not exactly 100%); L is the remaining round-trip dissipative optical loss; S_g and S_s are, respectively, the beam cross-sectional areas of the fundamental in the gain medium and in the saturable absorber; and γ is the inversion reduction factor, which actually corresponds to the net reduction in the population inversion that results from the stimulated emission of a single photon.

Equations (9)–(12) are valid for an arbitrary intracavity frequency-doubled passively Q-switched laser when the second harmonic is coupled out in two opposite directions. If there is a difference between the beam cross sections of the fundamental in the gain medium and in the nonlinear crystal, $\phi(r, t)$ in the last term on the right-hand side of Eq. (9) should be changed to $(S_g/S_n)\phi(0,t)\exp(-2r^2 S_g/\omega_L{}^2 S_n)$, where S_g/S_n is the ratio of the beam cross section of the fundamental in the gain medium to that in the nonlinear crystal. If the laser is end pumped by another laser (for example, by a LD or a

Ti:sapphire laser), the initial population inversion density $n(r, 0)$ can be assumed to be a Gaussian transversal distribution.[13,14] If the laser is side pumped by LDs or by a flash lamp it is reasonable to consider $n(r,0)$ to be uniform, which corresponds to the case of a Gaussian transversal distribution with the pump size approaching infinity. Before the laser action begins, all the saturable-absorber population is situated in the ground state. So the initial value of the ground-state population densities of the saturable absorber ${n_{sg}}^{(1)}(r, t)$ and ${n_{sg}}^{(2)}(r, t)$ can be considered to be n_{s0}. The initial photons come from spontaneous-emission noise. When the rate equations are solved numerically, $\phi(r, 0)$ can be set at a value much smaller than the peak value of the photon density $\phi_m(r, t)$ [for example, $\phi(r, 0) = 10^{-4}\ \phi_m(r, t)$]. If $\phi(r, 0)$ is even smaller, the pulse buildup time will become longer but the pulse energy and the pulse width will not change.[14] Therefore the initial conditions for intracavity frequency-doubled passively Q-switched lasers are as follows:

$$ {n_{sg}}^{(1)}(r, 0) = {n_{sg}}^{(2)}(r, 0) = n_{s0}, \tag{13} $$

$$ \phi(r, 0) \approx 10^{-4}\ \phi_m(r, t), \tag{14} $$

$$ n(r, 0) = n(0, 0)\exp\left(-\frac{2r^2}{{\omega_p}^2}\right), \tag{15} $$

where ω_p is the average radius of the pump beam in the gain medium and $n(0,0)$ is the initial population inversion density in the laser axis. Inasmuch as laser action begins at the moment that the population inversion density crosses the initial threshold value in a passively Q-switched laser, by substituting Eqs. (3), (10)–(13), and (15) into Eq. (9) and setting $\int_0^\infty [\mathrm{d}\phi(r, t)/\mathrm{d}t] 2\pi r \mathrm{d}r = 0$ and $t = 0$, we can determine the initial population inversion density in the laser axis $n(0, 0)$:

$$ n(0, 0) = \frac{\ln(1/R) + 2\sigma_{\mathrm{gsa}} n_{s0} l_s + L}{2\sigma l}\left(1 + \frac{{\omega_L}^2}{{\omega_p}^2}\right). \tag{16} $$

C. Rate Equations with Low Second-Harmonic Generation Conversion Efficiency and Optimal Orientation of the Saturable Absorber

In most situations the saturable absorber should be in its optimal orientation and the SHG conversion efficiency belongs to the low regime. [This means that the single-pass SHG conversion efficiency $I_{\mathrm{SH}}(r, t)/I_F(r, t)$ is less than 20%.] Theoretically, the optimal orientation of the saturable absorber corresponds to $\zeta = 0,\ \pi/2,\ \pi,\ 3\pi/2$. When the single-pass SHG conversion efficiency $I_{\mathrm{SH}}(r, t)/I_F(r, t)$ is less than 20%, Eq. (1) and the last term on the right-hand side of Eq. (9), respectively, can be approximated by

$$ I_{\mathrm{SH}}(r, t) \approx \eta {I_F}^2(r, t), \tag{17} $$

$$ \int_0^\infty \frac{2\phi(r, t)}{t_r} \tanh^2[\eta^{1/2}(chv/2)^{1/2}\phi^{1/2}(r, t)] 2\pi r \mathrm{d}r \approx \int_0^\infty \frac{chv\eta}{t_r}\phi^2(r, t) 2\pi r \mathrm{d}r, \tag{18} $$

Thus, when the saturable absorber is in its optimal orientation (with $\zeta = 0$) and the SHG conversion efficiency belongs to the low regime, Eqs. (9) and (11) can be simplified as

$$ \begin{aligned} \int_0^\infty \frac{\mathrm{d}\phi(r, t)}{\mathrm{d}t} 2\pi r \mathrm{d}r &= \int_0^\infty \frac{\phi(r, t)}{t_r}[2\sigma n(r, t) l - \ln(1/R) - L] 2\pi r \mathrm{d}r \\ &\quad - \int_0^\infty \frac{\phi(r, t)}{t_r}\{2\sigma_{\mathrm{gsa}} {n_{sg}}^{(1)}(r, t) l_s + 2\sigma_{\mathrm{esa}} \\ &\quad \times [n_{s0} - {n_{sg}}^{(1)}(r, t)] l_s\} 2\pi r \mathrm{d}r \\ &\quad - \int_0^\infty \frac{chv\eta}{t_r}\phi^2(r, t) 2\pi r \mathrm{d}r, \end{aligned} \tag{19} $$

$$ \frac{\mathrm{d}{n_{sg}}^{(1)}(r, t)}{\mathrm{d}t} = -\frac{S_g}{S_s}\sigma_{\mathrm{gsa}} c\phi(r, t){n_{sg}}^{(1)}(r, t). \tag{20} $$

Equations (19), (20), and (10), as well as the initial conditions of expressions (13)–(16), constitute the rate equations for the intracavity frequency-doubled passively Q-switched laser with low SHG conversion efficiency and optimal orientation of the saturable absorber.

In Ref. 14 it was shown that the general solutions of the rate equations for a passively Q-switched laser (not an intracavity frequency-doubled laser) depend on three synthetic parameters and that one can estimate the pulse characteristics of an arbitrary passively Q-switched laser by substituting the specific parameters of the laser into the general solutions. Now we treat Eqs. (19), (20), and (10) as well as the initial conditions of expressions (13)–(16) in the same way as was done in Ref. 14. The steps are as follows: First, we obtain the relation between $n(r, t)$ and $\phi(r, t)$ and the relation between ${n_{sg}}^{(1)}(r, t)$ and $\phi(r, t)$ by substituting Eqs. (3), (13), (15), and (16) into Eqs. (10) and (20). Second, by substituting these two relations into Eq. (19), we obtain the basic differential equation that describes $\phi(0, t)$ as a function of t. Third, by normalizing some parameters and substituting the normalized parameters into the equation that describes $\mathrm{d}\phi(0, t)/\mathrm{d}t$, we obtain the differential equation that describes the normalized photon density versus the normalized time. Then we obtain the following equation:

$$ \begin{aligned} \frac{d\Phi(0, \tau)}{\mathrm{d}\tau} &= \Phi(0, \tau)\int_0^1 \exp[-A(\tau)y^\beta]\mathrm{d}y \\ &\quad - \left(1 - \frac{1}{N}\right)\Phi(0, \tau)\frac{1 - \exp[-\alpha A(\tau)]}{\alpha A(\tau)} \\ &\quad - \frac{\Phi(0, \tau)}{N} - \eta_{\mathrm{SHG}}\Phi^2(0, \tau), \end{aligned} \tag{21} $$

where τ is the normalized time and $\Phi(0, \tau)$ is the normalized photon density in the laser axis; τ, $\Phi(0, \tau)$, $A(\tau)$, β, α, N, and η_{SHG} are as follows:

$$\tau = \frac{t}{t_r}\left[\ln\left(\frac{1}{R}\right) + \ln\left(\frac{1}{{T_0}^2}\right) + L\right], \tag{22}$$

$$\Phi(0, \tau) = \phi(0, \tau)\frac{2\gamma\sigma l'}{\ln\left(\frac{1}{R}\right) + \ln\left(\frac{1}{{T_0}^2}\right) + L}, \tag{23}$$

$$A(\tau) = \int_0^\tau \Phi(0, \tau)\mathrm{d}\tau, \tag{24}$$

$$\beta = \frac{1}{1 + (\omega_L/\omega_p)^2}, \tag{25}$$

$$\alpha = \frac{\sigma_{\rm gsa}S_g}{\gamma\sigma S_s}, \tag{26}$$

$$N = \frac{\ln\left(\frac{1}{R}\right) + \ln\left(\frac{1}{{T_0}^2}\right) + L}{\ln\left(\frac{1}{R}\right) + \left(\frac{\sigma_{\rm esa}}{\sigma_{\rm gsa}}\right)\ln\left(\frac{1}{{T_0}^2}\right) + L}, \tag{27}$$

$$\eta_{\rm SHG} = \frac{h\upsilon\,\eta}{2\sigma\gamma t_r}, \tag{28}$$

where T_0 is the initial transmission of the saturable absorber; i.e.,

$$T_0 = \exp(-\sigma_{\rm gsa}n_{s0}l_s). \tag{29}$$

Equation (21) is just the basic differential equation that describes the normalized photon density in the laser axis versus the normalized time. It is suitable for intracavity frequency-doubled passively Q-switched lasers with low SHG conversion efficiency and optimal orientation of the saturable absorber. For the xenon flash-lamp-pumped passively Q-switched SFD Nd:GdCOB laser, the SHG conversion efficiency belongs to the low regime (see the analysis that follows). The solutions of Eq. (21) depend on four synthetic parameters: β, α, N, and $\eta_{\rm SHG}$. β is related to ω_p/ω_L [seen in Eq. (25)]. α is a mark that indicates how easily the saturable absorber is bleached. The larger α is, the more easily the saturable absorber is bleached.[14,22,23] N is the ratio of the initial population inversion density to the threshold population inversion density in the case of $\alpha \rightarrow \infty$.[14] The product of $\eta_{\rm SHG}$ and $\Phi^2(0, \tau)$ is the SHG-caused loss rate of the normalized photon density in the laser axis $\Phi(0, \tau)$ with respect to normalized time τ. Considering that η is a parameter to mark the ability of the nonlinear crystal to convert the fundamental to the SH and that the normalizing factor of τ is proportional to t_r [shown in Eq. (22)], it is easy to understand that $\eta_{\rm SHG}$ is directly proportional to η and inversely proportional to t_r.

D. Comparison of Theoretical and Experimental Results; Discussion

α is determined mainly by the ratio of the saturable-absorber ground-state absorption cross section to the gain-medium stimulated-emission cross section [shown in Eq. (26)]. The ground-state and excited-state absorption cross sections of Cr^{4+}:YAG saturable absorbers, $\sigma_{\rm gsa}$ and $\sigma_{\rm esa}$, have been measured by many authors,[18–20,24–27] and the reported values scatter in a broad range. Maybe the Cr^{4+}:YAG saturable absorbers from different producers have some differences in $\sigma_{\rm gsa}$ and $\sigma_{\rm esa}$ because of some differences in the growing conditions. Nevertheless, most of the reported values of $\sigma_{\rm gsa}$ are of the same order of magnitude ($10^{-18}\,\mathrm{cm}^2$). Our measurement result is $4.3 \times 10^{-18}\,\mathrm{cm}^2$,[24] situated in the middle of the reported values. The stimulated-emission cross sections of the Nd:GdCOB crystal with the fundamental-frequency emission polarizing along crystallophysic axes X, Y, and Z are measured to be, respectively, $\sigma_X = 4.2 \times 10^{-20}\,\mathrm{cm}^2$, $\sigma_Y = 2.1 \times 10^{-20}\,\mathrm{cm}^2$, and $\sigma_Z = 1.9 \times 10^{-20}\,\mathrm{cm}^2$.[1,3] For Nd:GdCOB crystal cut at $\theta = 66.8°$ and $\varphi = 132.6°$, the polarization of the fundamental-frequency emission is not parallel to any of the three principal axes. But it is reasonable to consider that the stimulated-emission cross section σ is not far from σ_X, σ_Y, and σ_Z. Thus the ratio of $\sigma_{\rm gsa}$ to σ will be of the order of 100. Considering that inversion reduction factor γ and S_g/S_s are not far from 1, the value of α for the Cr^{4+}:YAG passively Q-switched SFD Nd:GdCOB laser is also of the order of 100. For a passively Q-switched laser, when α is larger than 10, the situation is close to that when $\alpha \rightarrow \infty$.[14,22,23] Therefore, for the Cr^{4+}:YAG passively Q-switched SFD Nd:GdCOB laser we can set $\alpha \rightarrow \infty$ when Eq. (21) is solved numerically.

Because the Nd:GdCOB laser is pumped by a flash lamp, the initial population inversion density can be considered to be uniform. This is equivalent to the Gaussian transversal distribution when $\omega_p/\omega_L \rightarrow \infty$ (i.e., $\beta \rightarrow 1$), and the integral in the first term on the right-hand side of Eq. (21) can be calculated. Thus the equation that describes the operation of the flash-lamp-pumped Cr^{4+}:YAG passively Q-switched SFD Nd:GdCOB laser is simplified as

$$\frac{\mathrm{d}\Phi(0, \tau)}{\mathrm{d}\tau} = \Phi(0, \tau)\frac{1 - \exp[-A(\tau)]}{A(\tau)} - \frac{\Phi(0, \tau)}{N} - \eta_{\rm SHG}\Phi^2(0, \tau). \tag{30}$$

Of course Eq. (30) is also suitable for other flash-lamp-pumped passively Q-switched lasers with large α, low SHG conversion efficiency, and optimal orientation of the saturable absorber. The solutions of Eq. (30) depends on only two synthetic parameters: N and $\eta_{\rm SHG}$. By solving Eq. (30) numerically we can obtain the relation between $\Phi(0, \tau)$ and τ and the relation between $\Phi^2(0, \tau)$ and τ for various values of N and $\eta_{\rm SHG}$. From the relation between $\Phi^2(0, \tau)$ and τ we can obtain $\Delta\tau_{\rm SH}$ and $e_{\rm SH}$, where $\Delta\tau_{\rm SH}$ is the width (FWHM) of $\Phi^2(0, \tau)$ and $e_{\rm SH}$ is the product of $\eta_{\rm SHG}$ and the integral of $\Phi^2(0, \tau)$ over τ from zero to infinity; i.e.,

$$e_{\rm SH} = \eta_{\rm SHG}\int_0^\infty \Phi^2(0, \tau)\mathrm{d}\tau. \tag{31}$$

The instantaneous output power $P_{\rm SHout}(\tau)$ and the output pulse energy $E_{\rm SHout}$ of the SH can be written as

$$P_{\mathrm{SHout}}(\tau) = \eta_{\mathrm{out}} h v l' \int_0^\infty \frac{\mathrm{d}\phi(r,t)}{\mathrm{d}t}\bigg|_{\mathrm{SHG}} 2\pi r \mathrm{d}r$$
$$= \frac{\pi {\omega_L}^2}{8} \eta_{\mathrm{out}} \eta (chv)^2 \phi^2(0,t)$$
$$= \frac{\pi {\omega_L}^2 hv}{4\sigma\gamma t_r}\left[\ln\left(\frac{1}{R}\right) + \ln\left(\frac{1}{{T_0}^2}\right) + L\right]^2$$
$$\times\ \eta_{\mathrm{out}} \eta_{\mathrm{SHG}} \Phi^2(0,\tau), \tag{32}$$

$$E_{\mathrm{SHout}} = \int_0^\infty P_{\mathrm{SHout}}(t)\mathrm{d}t$$
$$= \frac{\pi {\omega_L}^2}{8} \eta_{\mathrm{out}} \eta (chv)^2 \int_0^\infty \phi^2(0,t)\mathrm{d}t$$
$$= \frac{\pi {\omega_L}^2 hv}{4\sigma\gamma}\left[\ln\left(\frac{1}{R}\right) + \ln\left(\frac{1}{{T_0}^2}\right) + L\right]$$
$$\times\ \eta_{\mathrm{out}} e_{\mathrm{SH}}, \tag{33}$$

where η_{out} is a factor that represents the ratio of output power to the total power generated by SHG. Because the instantaneous output power of the SH is proportional to $\Phi^2(0, \tau)$, its pulse width W_{SH} can be written as

$$W_{\mathrm{SH}} = \frac{t_r \Delta\tau_{\mathrm{SH}}}{\ln\left(\frac{1}{R}\right) + \ln\left(\frac{1}{{T_0}^2}\right) + L}. \tag{34}$$

Figures 7 and 8 show, respectively, the variations of e_{SH} and $\Delta\tau_{\mathrm{SH}}$ as functions of N for several values of η_{SHG}. Figures 9 and 10 show, respectively, the variations of e_{SH} and $\Delta\tau_{\mathrm{SH}}$ as functions of η_{SHG} for various values of N. As can be seen from Figs. 7 and 9, for a given η_{SHG}, e_{SH} increases monotonically with increasing N. For a given N, e_{SH} increases monotonically with increasing η_{SHG}, and the derivative of e_{SH} with respect to η_{SHG} decreases monotonically with increasing η_{SHG}; i.e., e_{SH} approaches a certain value when η_{SHG} becomes large enough. As can be seen from Figs. 8 and 10, for a given η_{SHG}, $\Delta\tau_{\mathrm{SH}}$ initially

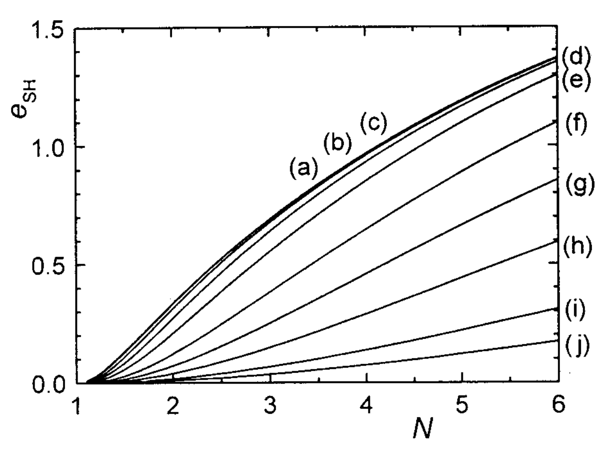

Fig. 7. Relation between e_{SH} and N for several values of η_{SHG}: (a) $\eta_{\mathrm{SHG}} = 10$, (b) $\eta_{\mathrm{SHG}} = 5$, (c) $\eta_{\mathrm{SGH}} = 2$, (d) $\eta_{\mathrm{SHG}} = 1$, (e) $\eta_{\mathrm{SHG}} = 0.5$, (f) $\eta_{\mathrm{SHG}} = 0.2$, (g) $\eta_{\mathrm{SHG}} = 0.1$, (h) $\eta_{\mathrm{SHG}} = 0.05$, (i) $\eta_{\mathrm{SHG}} = 0.02$, (j) $\eta_{\mathrm{SHG}} = 0.01$. (a)–(c) nearly overlap.

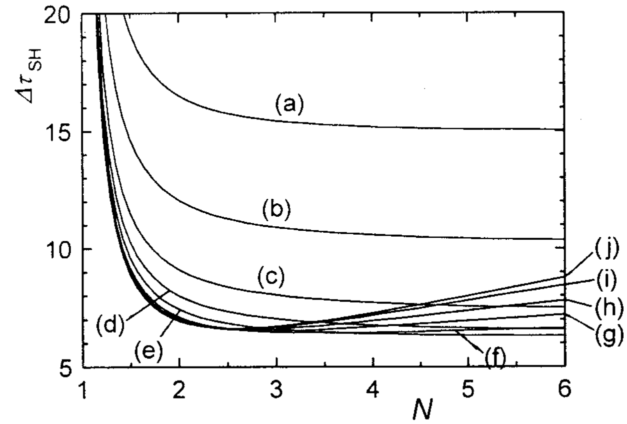

Fig. 8. Relation between $\Delta\tau_{\mathrm{SH}}$ and N for several values of η_{SHG}: (a) $\eta_{\mathrm{SHG}} = 10$, (b) $\eta_{\mathrm{SHG}} = 5$, (c) $\eta_{\mathrm{SHG}} = 2$, (d) $\eta_{\mathrm{SHG}} = 1$, (e) $\eta_{\mathrm{SHG}} = 0.5$, (f) $\eta_{\mathrm{SHG}} = 0.2$, (g) $\eta_{\mathrm{SHG}} = 0.1$, (h) $\eta_{\mathrm{SHG}} = 0.05$, (i) $\eta_{\mathrm{SHG}} = 0.02$, (j) $\eta_{\mathrm{SHG}} = 0.01$.

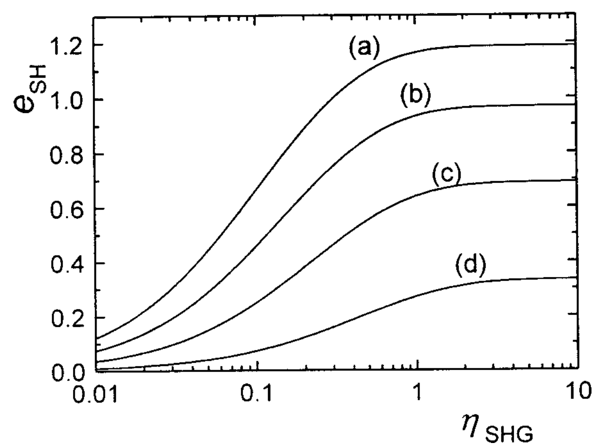

Fig. 9. Relation between e_{SH} and η_{SHG} for four values of N: (a) $N = 5$, (b) $N = 4$, (c) $N = 3$, (d) $N = 2$.

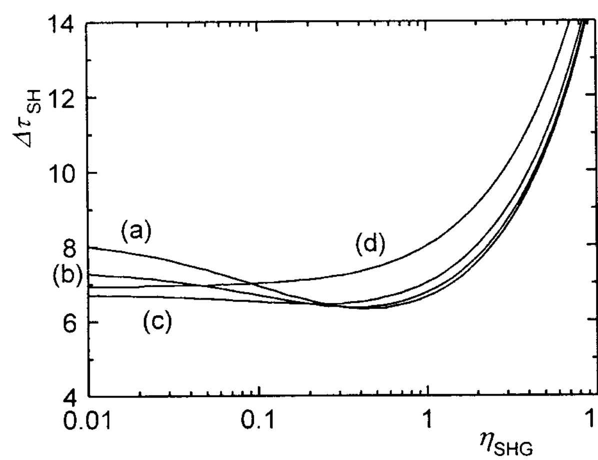

Fig. 10. Relation between $\Delta\tau_{\mathrm{SH}}$ and η_{SHG} for several values of N: (a) $N = 5$, (b) $N = 4$, (c) $N = 3$, (d) $N = 2$.

decreases steeply to a minimum value and then increases slightly with increasing N; and the larger η_{SHG} is, the larger N_0 is, where N_0 is the value of N at which $\Delta\tau_{\mathrm{SH}}$ reaches its minimum value. For a given N, $\Delta\tau_{\mathrm{SH}}$ initially decreases to a minimum value and then increases with increasing $\eta_{\rm SHG}$; and the larger N is, the larger $\eta_{\rm SHG0}$ is, where $\eta_{\rm SHG0}$ is the value of $\eta_{\rm SHG}$ at which $\Delta\tau_{\rm SH}$ reaches its minimum value.

Because the Cr^{4+}:YAG saturable absorber has strong absorption for a 0.53-μm beam,[28,29] the 0.53-μm light passing through the Cr^{4+}:YAG saturable absorber is mostly all absorbed and the 0.53-μm output consists mainly of the light propagating toward the other direction. When the saturable absorber with $T_0 = 88\%$ is used, its transmission at 0.53 μm is only 37%, and $\eta_{\rm out}$ is estimated to be 68%. When $T_0 = 91\%$, the transmission of the saturable absorber at 0.53 μm is 47%, and $\eta_{\rm out}$ is estimated to be 73%.

Substituting $\sigma_{\rm gsa} = 4.3 \times 10^{-18}\,{\rm cm}^2$, $\sigma_{\rm esa} = 8.2 \times 10^{-19}\,{\rm cm}^2$,[24] $R = 0.4\%$, and $L = 3.8\%$ into Eq. (27), we obtain $N = 3.3$ for $T_0 = 88\%$ and $N = 3.0$ for $T_0 = 91\%$.

The value of $\eta_{\rm SHG}$ for the passively Q-switched SFD Nd:GdCOB laser is relatively difficult to obtain. The reasons are as follows: First, although the Nd:GdCOB crystal is placed at the center of the cavity, because of the thermal effect in the gain medium induced by the pumping the propagating direction of the light for $r \neq 0$ is not exactly parallel to the laser axis, and this will generate a phase mismatch. Second, the phase mismatch generated by the misalignment during the cutting of crystal is difficult to estimate. Third, owing to the walk-off effect, the effective length of the nonlinear crystal should be less than its real length, and this effective length for the Nd:GdCOB crystal is difficult to estimate.

It can be seen from Eq. (34) that $W_{\rm SH}$ depends only on $\eta_{\rm SHG}$ for given t_r, R, T_0, L, and N (these parameters are known), so we use $W_{\rm SH}$ in the case of $T_0 = 88\%$ to determine $\eta_{\rm SHG} = h\upsilon\eta/(2\sigma\gamma t_r)$. When $L_e = 36$ cm, $W_{\rm SH}$ is 91 ns. By using Eq. (34) and the data mentioned above we obtain $\Delta\tau_{\rm SH} = 10.8$. By solving Eq. (30) we obtain a value of $h\upsilon\eta/(2\sigma\gamma)$ that corresponds to $\Delta\tau_{\rm SH} = 10.8$ of 12.8 ns. When L_e has other values, the value of $h\upsilon\eta/(2\sigma\gamma)$ obtained is 11.8–14.1 ns, and the average value is 13.1 ns. Thus the value of $\eta_{\rm SHG}$ for various values of t_r can be written as

$$\eta_{\rm SHG} = \frac{h\upsilon\eta}{2\sigma\gamma t_r} = \frac{13.1}{t_r}, \tag{35}$$

where t_r is in nanoseconds. When L_e is 24–48 cm, the value of $\eta_{\rm SHG}$ is 7.6–4.0. Even when $\eta_{\rm SHG} = 10$ and $N = 3.3$, the peak value of the normalized photon density in the laser axis, Φ_m, is 0.0568. From expressions (4), (17), (23), and (28), we obtain $I_{\rm SH}(0, t_m)/I_F(0, t_m) = \eta_{\rm SHG}\Phi_m[\ln(1/R) + \ln(1/T_0{}^2) + L] = 0.17$, which is less than 0.2, where $I_{\rm SH}(0, t_m)$ is the intracavity peak intensity of the unidirectional SH in the laser axis and $I_F(0, t_m)$ is the corresponding intensity of the fundamental. For other values of r and t, $I_{\rm SH}(r, t)/I_F(r, t)$ is smaller than $I_{\rm SH}(0, t_m)/I_F(0, t_m)$. Therefore Figs. 7–10 are suitable for describing a Cr^{4+}:YAG passively Q-switched SFD Nd:GdCOB laser.

When cavity length L_e is changed while the other experimental conditions are fixed, the value of $\eta_{\rm SHG}$ and the radius of the beam at the gain medium are also changed. $\eta_{\rm SHG}$ is changed according to Eqs. (8) and (35), and the beam radius is changed according to the following relation:

$$\omega_L{}^4 = \left(\frac{\lambda}{\pi}\right)^2 \frac{(l'/2)(2f)^2(R_e - l'/2)}{(2f - l'/2)(R_e + 2f - l'/2)}, \tag{36}$$

where λ is the wavelength of the fundamental, R_e is the radius of curvature of the two cavity mirrors, and f is the equivalent focal length of the thermal lens in the Nd:GdCOB crystal induced by pumping. We calculate the value of f by using the parameters of the resonator and the measured beam size and divergence of the fundamental, and f depends on the pump energy. When $T_0 = 88\%$, the pump pulse energy is 8.6 J and f is 2.5 m. When $T_0 = 91\%$, the pump pulse energy is 6.8 J and f is 3.2 m.

To calculate the pulse energy we need to know the product of σ and γ [shown by Eq. (33)]. Because all the other parameters for calculating the pulse energy have been obtained, we use the experimental results of the pulse energy in the case of $T_0 = 88\%$ to determine $\sigma\gamma$. When $L_e = 36$ cm, $e_{\rm SH}$ is 0.779 and $E_{\rm SHout}$ is 2.43 mJ. According to Eq. (33), $\sigma\gamma$ is determined to be $1.42 \times 10^{-20}\,{\rm cm}^2$. When L_e has other values, the value of $\sigma\gamma$ obtained is 1.38×10^{-20} to $1.51 \times 10^{-20}\,{\rm cm}^2$, and the average value is $1.44 \times 10^{-20}\,{\rm cm}^2$.

The solid curves in Fig. 4 are obtained from $\sigma\gamma = 1.44 \times 10^{-20}\,{\rm cm}^2$, the relations shown in Figs. 7 and 9, and Eqs. (33), (35), and (36). It can be seen from Fig. 4 that the pulse energy increases slightly with L_e. The reasons are that $e_{\rm SH}$ remains nearly constant when $\eta_{\rm SHG}$ is 7.6–4.0 for a given N (Figs. 7 and 9) and that ω_L increases slightly with L_e when L_e is 24–48 cm. The solid curves in Fig. 5 are obtained from Eqs. (34) and (35) and the relations shown in Figs. 8 and 10. Because the curves in Figs. 8 and 10 are obtained when $\alpha \to \infty$, the pulse width is independent of γ, σ, and the beam radius.

To account for the dependence of the pulse energy and width on δ, we must use the rate equations including the anisotropy of the saturation process of the saturable absorber, which are not so easy to simplify as Eqs. (19), (20), and (10) can be simplified into Eq. (21). The solid curves in Figs. 2 and 3 are obtained by solution of expressions (9)–(12) numerically. In solving these equations we use $\sigma\gamma = 1.44 \times 10^{-20}\,{\rm cm}^2$ and $\eta = 2.02 \times 10^{-9}\,{\rm cm}^2\,{\rm W}^{-1}$ [which is obtained from Eq. (35)]. The other necessary parameters include $S_g/S_n = 1$, $n_{s0} = 4.51 \times 10^{17}\,{\rm cm}^{-3}$,[24] $l_s = 0.66$ mm (for $T_0 = 88\%$), $l_s = 0.49$ mm (for $T_0 = 91\%$), $2\sigma ln(0,0) = 0.30$ (for $T_0 = 88\%$), and $2\sigma ln(0,0) = 0.23$ [for $T_0 = 91\%$, $2\sigma ln(0,0)$ can be used as one parameter in solving the equations].

It can be seen from Figs. 2–5 that the theoretical results are in fair agreement with the experimental results. It can also be seen from Figs. 4 and 5 that there are some differences between the theoretical results and the experimental results when L_e is relatively large. The reasons may be as follows: First, in the theoretical analysis, the relaxation time with which the Cr^{4+} that has been excited to a higher level by excited-state absorption relaxes to the first excited state is assumed to be infinitely small and the population is assumed to be situated in either the ground state or the first excited state. Actually this relaxation time is of the order of 100 ps.[25] When the intracavity 1.06-μm intensity is high enough, the higher level above the first excited state can also be populated. The absorption transition and the relaxation between the first excited state and the higher level lead to modulation of Q-switched laser pulse. The time interval between two successive modulation pulses is equal to the round-trip transit time of the light in the cavity. The actual Q-switched pulse seems to be the overlap of the Q-switched pulse and small mode-locked pulses (shown in Fig. 6). This modulation consumes some of the inversion population and makes the pulse energy be less than the expected value. Second, L should increase slightly with the cavity length, which we did not consider in the theoretical analysis.

4. CONCLUSION

We have demonstrated the performance of a flash-lamp-pumped passively Q-switched SFD Nd:GdCOB laser with Cr^{4+}:YAG saturable absorbers. When the initial transmission of the Cr^{4+}:YAG saturable absorber is 88% and the cavity length is 48 cm, 0.53-μm pulses with an energy of 2.6 mJ and a width of 112 ns are obtained. When $T_0 = 88\%$ and $L_e = 24$ cm, the pulse energy is 2.1 mJ, the pulse width is 71 ns, and the corresponding peak power and peak intensity are 29 kW and 15 MW/cm^2, respectively. Because the Cr^{4+}:YAG saturable absorber has a low transmission at the SH wavelength,[28,29] it constitutes a large loss to the SH. If a mirror that is coated for high reflection at the SH wavelength and for high transmission at the fundamental wavelength is placed between the SFD crystal and the saturable absorber such that the SH does not pass through the saturable absorber, a larger SH pulse energy is expected to be obtained.

Theoretically, we have taken the transversal distribution of the intracavity photon density into account in the rate equations for an intracavity frequency-doubled passively Q-switched laser, and we used the solutions to account for the behavior of the passively Q-switched Nd:GdCOB laser. Equations (9)–(12), as well as the initial conditions of expressions (13)–(16), are suitable for an arbitrary intracavity-frequency-doubled passively Q-switched laser when the SH is coupled out in two opposite directions. When the saturable absorber is in its optimal orientation and the SHG conversion efficiency is in the low regime, Eqs. (19), (20), and (10), as well as the initial conditions of expressions (13)–(16), constitute the rate equations. We have shown by normalizing the related parameters that the general solutions depend on four synthetic dimensionless parameters: β, α, N, and η_{SHG}, and the dependence is determined by Eq. (21). Equation (30), as well as the curves in Figs. 7–10, is suitable for flash-lamp-pumped intracavity frequency-doubled passively Q-switched lasers with large α, low SHG conversion efficiency, and optimal orientation of the saturable absorber. We do not believe that all possible applications of these space-dependent rate equations have been fully explored in this paper. We believe that there are potential applications in the analysis of LD-pumped intracavity frequency-doubled passively Q-switched lasers[30–32] because these rate equations can be used for analysis of the dependence of the pulse characteristics on ω_p/ω_L (or β).

ACKNOWLEDGMENTS

This research is partly supported by the National Science Foundation of China and the Science Foundation of Shandong Province.

X. Zhang's e-mail address is zhangxingyu@hotmail.com.

REFERENCES

1. F. Mougel, G. Aka, A. Kahn-Harari, H. Hurbert, J. M. Benitez, and D. Vivien, "Infrared laser performance and self-frequency doubling of Nd^{3+}:$Ca_4GdO(BO_3)_3$ (Nd:GdCOB)," Opt. Mater. **8**, 161–173 (1997).
2. D. Vivien, F. Mougel, G. Aka, A. Kahn-Harari, and D. Pelenc, "Neodymium-activated $Ca_4GdB_3O_{10}$ (Nd:GdCOB): a multifunctional material exhibiting both laser and nonlinear optical properties," Laser Phys. **8**, 759–753 (1998).
3. F. Mougel, F. Auge, G. Aka, A. Kahn-Harari, D. Vivien, F. Balembois, P. Georges, and A. Brun, "New green self-frequency-doubling diode-pumped Nd^{3+}:$Ca_4GdO(BO_3)_3$ laser," Appl. Phys. B **67**, 533–535 (1998).
4. S. Zhang, Z. Cheng, J. Han, G. Zhou, Z. Shao, C. Wang, Y. T. Chow, and H. Chen, "Growth and investigation of efficient self-frequency-doubling $Nd_xGd_{1-x}Ca_4O(BO_3)_3$ crystal," J. Cryst. Growth **206**, 197–202 (1999).
5. C. Wang, Y. T. Chow, W. A. Gambling, S. Zhang, Z. Cheng, Z. Shao, and H. Chen, "Efficient self-frequency doubling of Nd:GdCOB crystal by type-I phase matching out of its principal planes," Opt. Commun. **174**, 471–474 (2000).
6. F. Auge, F. Mougel, F. Balembois, P. Georges, A. Brun, G. Aka, A. Kahn-Harari, and D. Vivien, "Efficient cw and Q-switch operation of a self-frequency-doubling diode-pumped Nd^{3+}:$Ca_4Gd_{1-x}Nd_xB_3O_{10}$ (Nd:GdCOB) crystal," in *Conference on Lasers and Electro-Optics (CLEO/U.S.)* (Optical Society of America, Washington, D.C., 1999), p. 530, paper CFF3.
7. W. G. Wagner and B. A. Lengyel, "Evolution of the giant pulse in a laser," J. Appl. Phys. **34**, 2040–2046 (1963).
8. A. Szabo and R. A. Stein, "Theory of laser giant pulsing by a saturable absorber," J. Appl. Phys. **36**, 1562–1566 (1965).
9. J. E. Murray and S. E. Harris, "Pulse lengthening via overcoupled internal second-harmonic generation," J. Appl. Phys. **41**, 609–613 (1970).
10. E. C. Honea, C. A. Ebbers, R. J. Beach, J. A. Speth, J. A. Skidmore, M. A. Emanuel, and S. A. Payne, "Analysis of an intracavity-doubled diode-pumped Q-switched Nd:YAG laser producing more than 100 W of power at 0.532 μm," Opt. Lett. **23**, 1203–1205 (1998).
11. T. T. Kajava and A. L. Gaeta, "Intra-cavity frequency-doubling of a Nd:YAG laser passively Q-switched with GaAs," Opt. Commun. **137**, 93–97 (1997).
12. J. Liu and D. Kim, "Optimization of intracavity doubled passively Q-switched solid-state lasers," IEEE J. Quantum Electron. **35**, 1724–1730 (1999).
13. X. Zhang, S. Zhao, Q. Wang, B. Ozygus, and H. Weber, "Modeling of diode-pumped actively Q-switched lasers," IEEE J. Quantum Electron. **35**, 1912–1918 (1999).
14. X. Zhang, S. Zhao, Q. Wang, B. Ozygus, and H. Weber, "Modeling of passively Q-switched lasers," J. Opt. Soc. Am. B **17**, 1166–1175 (2000).
15. X. Zhang, S. Zhao, Q. Wang, L. Sun, S. Zhang, G. Yao, and Z. Zhang, "Laser diode pumped Cr^{4+}:YAG passively Q-switched Nd^{3+}:SFAP laser," Opt. Commun. **155**, 55–60 (1998).

16. W. Koechner, *Solid State Laser Engineering*, 4th ed. (Springer-Verlag, Berlin, 1996), Chap. 10.
17. J. J. Degnan, "Theory of the optimally coupled Q-switched laser," IEEE J. Quantum Electron. **25**, 214–220 (1995).
18. H. Eilers, K. R. Hoffman, W. M. Denis, S. M. Jacobson, and W. M. Yen, "Saturation of 1.064 μm absorption in Cr, Ca:$Y_3Al_5O_{12}$ crystals," Appl. Phys. Lett. **61**, 2958–2960 (1992).
19. P. Yankov, "Cr^{4+}:YAG Q-switching of Nd:host laser oscillators," J. Phys. D **27**, 1118–1120 (1994).
20. S. Camacho-Lopez, R. P. M. Green, G. J. Crofts, and M. J. Damzen, "Intensity-induced birefringence in Cr^{4+}:YAG," J. Mod. Opt. **44**, 209–219 (1997).
21. A. V. Kir'yanov, V. Aboites, and I. V. Mel'nikov, "Second-harmonic generation by Nd^{3+}:YAG/Cr^{4+}:YAG-laser pulses with changing state of polarization," J. Opt. Soc. Am. B **17**, 1657–1664 (2000).
22. J. J. Degnan, "Optimization of passively Q-switched lasers," IEEE J. Quantum Electron. **31**, 1890–1901 (1995).
23. X. Zhang, S. Zhao, Q. Wang, Q. Zhang, L. Sun, and S. Zhang, "Optimization of Cr^{4+}-doped saturable-absorber Q-switched lasers," IEEE J. Quantum Electron. **33**, 2286–2294 (1997).
24. X. Zhang, S. Zhao, Q. Wang, S. Wang, L. Sun, S. Zhang, G. Yao, and Z. Zhang, "Measurement of absorption cross section and ground state recovery time of Cr^{4+}-doped saturable absorber," J. Optoelectron. Laser **9**, 453–457 (1998) (in Chinese).
25. A. Suda, A. Kadoi, K. Nagasaka, H. Tashiro, and K. Midorikawa, "Absorption and oscillation characteristics of a pulsed Cr^{4+}:YAG laser investigated by a double-pulse pumping technique," IEEE J. Quantum Electron. **35**, 1548–1553 (1999).
26. G. Xiao, J. H. Lim, S. Yang, E. Van Stryland, M. Bass, and L. Weichman, "Z-scan measurement of the ground and excited state absorption cross sections of Cr^{4+} in yttrium aluminum garnet," IEEE J. Quantum Electron. **35**, 1086–1091 (1999).
27. Z. Burshtein, P. Blau, Y. Kalisky, Y. Shimony, and M. R. Kokta, "Excited-state absorption studies of Cr^{4+} ions in several garnet host crystals," IEEE J. Quantum Electron. **34**, 292–299 (1998).
28. H. Eilers, W. M. Dennis, W. M. Yen, S. Küch, K. Peterman, G. Huber, and W. Jia, "Performance of a Cr:YAG laser," IEEE J. Quantum Electron. **29**, 2508–2512 (1993).
29. H. Eilers, U. Hömmerich, S. M. Jacobsen, W. M. Yen, K. R. Hoffman, and W. Jia, "Spectroscopy and dynamics of Cr^{4+}:$Y_3Al_5O_{12}$," Phys. Rev. B **49**, 15,505–15,513 (1994).
30. W. G. Ostroumov, F. Heine, S. Kück, G. Huber, V. A. Mikhailov, and I. A. Shcherbakov, "Intracavity frequency-doubled diode-pumped Nd:$LaSc_3(BO_3)_4$ lasers," Appl. Phys. B **64**, 301–305 (1997).
31. Y. F. Chen, "Passive Q-switching of an intracavity frequency-doubled diode-pumped Nd:YVO_4/KTP green laser with Cr^{4+}:YAG," IEEE Photon. Technol. Lett. **9**, 1481–1483 (1997).
32. J. Bartschke, K.-J. Boller, R. Wallenstein, I. V. Klimov, V. B. Tsvetkov, and I. A. Shcherbakov, "Diode-pumped passively Q-switched self-frequency-doubling Nd:YAB laser," J. Opt. Soc. Am. B **14**, 3452–3456 (1997).